frontiers | Frontiers in Marine Science

TYPE Original Research
PUBLISHED 07 December 2023
DOI 10.3389/fmars.2023.1335064

OPEN ACCESS

EDITED BY
Chengji Shen,
Hohai University, China

REVIEWED BY
Gang Yang,
Nanjing University of Information Science and Technology, China
Yuwei Hu,
Chinese Academy of Sciences (CAS), China
Zhang Bo,
Shandong University of Science and Technology, China

*CORRESPONDENCE
Ye Ma
ye.mawater@outlook.com

RECEIVED 08 November 2023
ACCEPTED 24 November 2023
PUBLISHED 07 December 2023

CITATION
Wang Q, Ma Y, Cheng Z and Du Y (2023) Coastline changes under natural and anthropogenic drivers in a macro-tidal estuary between 2000-2020.
Front. Mar. Sci. 10:1335064.
doi: 10.3389/fmars.2023.1335064

Coastline changes under natural and anthropogenic drivers in a macro-tidal estuary between 2000-2020

Qian Wang[1], Ye Ma[1,2]*, Zhixin Cheng[1,2] and Yixiao Du[1]

[1]College of Environmental Science and Engineering, Dalian Maritime University, Dalian, Liaoning, China, [2]Centre for Ports and Maritime Safety, Dalian Maritime University, Dalian, Liaoning, China

Coastline changes in estuarine areas can result from a combination of natural processes such as erosion, sedimentation, and sea-level rise, as well as human activities, including urbanization and infrastructure development. These changes have the potential to affect the local environment, including submarine groundwater discharge, wetlands, and navigation routes. The Yalu River Estuary (YRE), situated on the border between China and North Korea, has been experiencing significant changes in its coastline over recent years. This study aims to investigate the coastline dynamics in the YRE from 2000 to 2020. The study employs Landsat 5/7/8 satellite data and proposes a modified Normalized Difference Water Index (NDWI) to accurately delineate the coast boundary, particularly in areas with extensive tidal flats like the YRE. The research findings indicate that from 2010 to 2020, significant changes occurred in the YRE shoreline, with erosion being the dominant trend. Human activities and alternations in hydrological conditions are important factors affecting the YRE coastline changes, contributing to the formation of distinctive spatiotemporal patterns. An extreme flooding event in the year 2010 also altered the inner estuarine coastline in the YRE, indicating the impact of strong natural drivers. Findings from this study provide a comprehensive understanding of the evolving coastal environment, considering natural and anthropogenic drivers, and highlight the importance of continuous monitoring in a region of ecological and geopolitical significance.

KEYWORDS

coastline, tidal estuary, satellite image, human impacts, image processing

1 Introduction

The coastline serves as a critical interface between land and the ocean, holding significant importance for both marine and terrestrial ecosystems, as well as human activities (Barbier et al., 2011). The study of coastline changes provides valuable insights into the dynamic interactions between the ocean and land, enabling the prediction of coastal erosion trends,

assessment of land degradation, and evaluation of the effectiveness of marine and coastal management strategies (Alesheikh et al., 2007). These changes are closely linked to natural phenomena such as climate change, sea-level rise, and river erosion, making coastline analysis an essential indicator of environmental transformations (Sánchez-Arcilla et al., 2016). Therefore, investigating coastline changes is crucial for the preservation of marine and coastal ecosystems, as well as the development of sustainable marine policies and management strategies.

Furthermore, human activities have exerted extensive influences on estuarine environments and coastlines. Various factors, including the overexploitation of river water resources, land development, and modifications to channels, have altered the sediment-carrying capacity of rivers, resulting in sedimentation and erosion in estuaries (Zhu et al., 2017; Xu et al., 2019). Additionally, activities such as port construction, coastal protection measures, and changes in coastal land use have significant impacts on coastlines, leading to coastal erosion, beach erosion, and ecosystem degradation (Turner et al., 1998). Along the entire coastal area of China, the most significant changes have occurred along the Bohai Sea coast. The proportion of artificial coastlines expanded from approximately 42.4% in 1990 to 81.5% in 2019 (Tian et al., 2020). Human activities have dominantly influenced the transport and the supply of sediment in coastal regions. This has led to the transformation of naturally meandering coastlines into straighter and more geometrically uniform artificial shorelines, resulting in a reduction of the overall length of these coastlines (Hapke et al., 2013).These anthropogenic activities pose potential threats to coastal populations, economies, and ecosystems. The anthropogenic activities on the changes of coastline could be a controlling factor for the development of the aquaculture industry, which can enhance food production and boost economic growth in coastal and rural communities. The natural irregular coastline is a crucial factor influencing water exchange between coastal regions and the open ocean, creating micro-environments with oceanographic conditions that sustain unique ecosystems for the local marine farming industry (Quiñones et al., 2019). Furthermore, anthropogenic activities, such as dredging, can disrupt the natural sediment balance along coastlines. Such changes can lead to coastal erosion, negatively impacting coastal infrastructure and potentially requiring costly mitigation measures, which could be involved with relatively high costs (Bianchini et al., 2019).

Two major methods have been widely used for coastline extraction (Muttitanon and Tripathi, 2005), with the regards of remote sensing image processing. The methods are the post-classification change detection approach and the direct spectral comparison approaches. The post-classification change detection approach involves comparing classified images from different time periods to identify and analyse land cover changes (Sahin et al., 2022). However, it is important to note that the accuracy of the data obtained through this approach is limited, and the accuracy generally depends on the precision of land cover classification in the study area, thereby resulting in larger deviations (Morgan and Hodgson, 2021). In contrast, the direct spectral comparison approach involves comparing the original data images through a series of algorithmic transformations to obtain comparative results (Zhang et al., 2013). Nevertheless, the direct spectral comparison approach is constrained by limitations such as lower spatial resolution and susceptibility to environmental factors, such as waves and tides. This precision could be even worse in areas with intensive tidal flats, a reliable method for coastline extraction in such area requires further exploration.

The Yalu River Estuary (YRE), a region of ecological and geopolitical significance on the China-North Korea border, has been subjected to substantial coastline changes over the years. The YRE features an irregular coastline, encompassing diverse landscapes, including underwater tidal ridges downstream, a delta plain in the estuary, and extensive tidal flats (Gao et al., 2012). Construction of upstream reservoirs has significantly decreased sediment supply and freshwater discharge, causing transformations in the river's West Branch, including its transition from a major waterway to a tidal inlet heavily impacted by siltation (Cheng et al., 2019). Large-scale reclamations have been conducted in the West Branch, accompanied by continuous dredging activities in Dandong Harbour's deep navigation channel (Cheng et al., 2020). While previous studies documented the coastline dynamics up to 2010 before the construction of the harbour, this research aims to bridge the gap by investigating coastline changes in the YRE over two decades from 2000 to 2020.

In this study, we investigate coastline changes in the YRE due to natural and human activities, therefore, this study focuses on the investigations of the coastline dynamics in the YRE from 2000 to 2020 using Landsat 5/7/8 satellite data. By including a modified Normalized Difference Water Index (NDWI), processing results can be more accurate to reflect the coastline condition in this estuary with complex tidal flats. Our findings provide a comprehensive understanding of the evolving coastal environment, considering natural and anthropogenic drivers, and highlight the importance of continuous monitoring in a region of ecological and geopolitical significance.

2 Methods

2.1 Study area

The Yalu River, originating from the Changbai Mountain in northeast China, flows between Dandong in the Liaoning Province of China and Sinuiju in North Korea, as shown in Figure 1. The Yalu River Estuary (YRE) is a vital coastal region that serves as a natural boundary between China and North Korea (Cheng et al., 2016). The area's coastline plays a crucial role in maintaining ecological balance and serving as a habitat for numerous species, and the YRE is a macro-tidal estuary with significant tidal variations. As reported by Bai et al. (2008), it exhibits an average tidal range of around 4.6 m, escalating to a maximum of approximately 6.7 m. The estuarine area displays a mix of tidal patterns. A consistent semi-diurnal tide is observed outside the estuary's entrance, while inside, the tide shifts to an irregular semi-diurnal pattern, influencing a tidal zone extending up to 54 km, as described by Yu et al. (2014). For areas with a macro-tidal range,

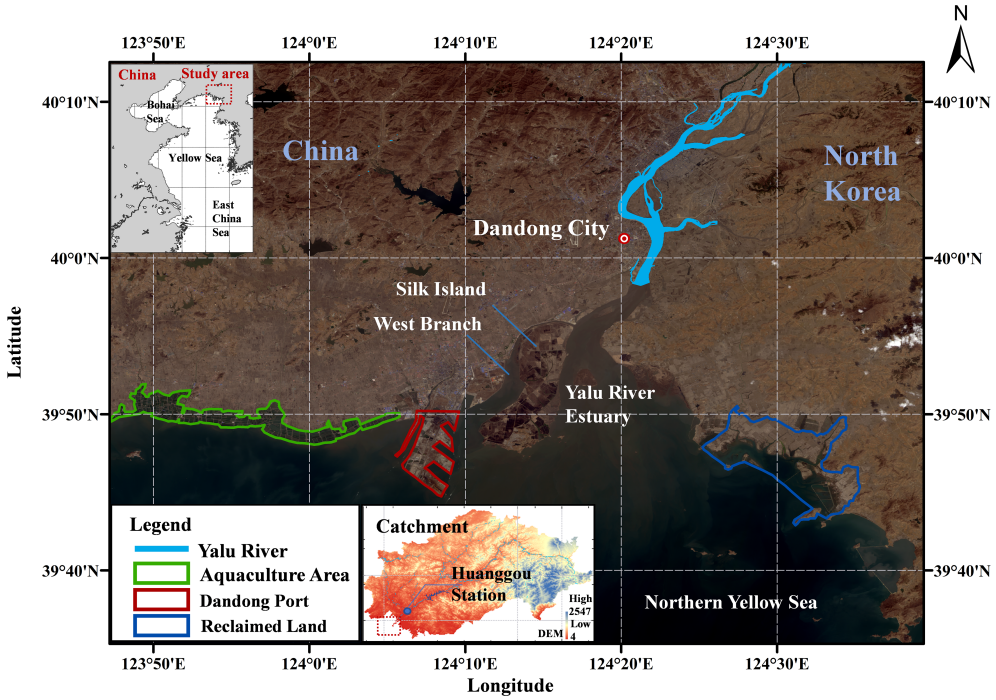

FIGURE 1
Satellite image of the study area in the Yalu River estuary, satellite image is from Landsat 8 OLI, and image was taken on April 10, 2020.

like the one in this study, the impact of tides on the coastline can lead to the increase of erosion or deposition. In turn, this macro-tide can significantly alter the coastline's shape. Furthermore, areas with smaller tidal ranges (micro tides: less than 2 meters, mesotides: 2-4 meters), wave action might play a more dominant role in shaping coastlines in these areas compared to macro-tidal regions. Due to strong coast erosion on the west bank of the river in China, the country has experienced significant land loss, resulting in a westward shift of the borderline from 1976 to 2010 (Li et al., 2012). To maintain the stability of this border, both the Chinese and North Korean governments have implemented various engineering projects, including dam construction and land reclamation.

The natural influences on coastline dynamics are profoundly affected by local hydrodynamic conditions, such as wave and current patterns, and particularly by the variations between high and low tides. Waves, particularly during high-energy events like storms, can erode beaches and dunes. Furthermore, the difference between high and low tides significantly influences the sediment movement and deposition along the coast. Coastline changes were corresponding with variations in the tidal range could reveal patterns of erosion and accretion. Large tide range can create extensive tidal flats, where areas that are periodically submerged and exposed, influencing sediment deposition and erosion patterns.

Thus, analysing coastline changes in this region is crucial for providing scientific guidance to both governments on this border-related issue.

The YRE region exhibits an irregular coastline with diverse landscapes, such as underwater tidal ridges downstream and a delta plain with a large-scale wetland in the estuary (Gao et al., 2012). Additionally, the region is distributed with extensive tidal flats. The construction of reservoirs upstream has led to a significant reduction in suspended sediment supply and freshwater discharge from the river (Shi et al., 2017). Specifically, the West Branch, which used to be the main waterway prior to these constructions, transformed into a tidal inlet and experienced substantial siltation thereafter. Extensive reclamation of tidal flats has occurred around Silk Island and Dandong Harbour in the West Branch, accompanied by continuous dredging in Dandong Harbour to maintain a deep navigation channel. These activities have altered the coastline and topography in the surrounding area, necessitating a comprehensive assessment of the associated impacts.

2.2 Satellite images

Satellite images from 2010 to 2020, applied in this study, were captured by the Landsat 5, 7, and 8 satellites, all of which are integral components of the United States NASA's Landsat program, the Landsat program has been providing images for nearly five decades (Roy et al., 2016). Specifically, Landsat 5 was equipped with a Multispectral Scanner and a Thematic Mapper, Landsat 7 featured an Enhanced Thematic Mapper Plus, and Landsat 8 was outfitted with an Operational Land Imager (OLI) and a Thermal Infrared Sensor (Zhu et al., 2016). Distinguished from other satellites, the Landsat series boasts several unique features: a sun-synchronous polar orbit, relatively low orbital altitude, rapid orbital cycles, multispectral sensor data acquisition, and imagery of varying resolutions. These attributes enable the Landsat satellites to provide high-quality, continuous, and global earth observation

data. Furthermore, the Landsat collections includes imagery that has undergone radiometric and geometric corrections (Dwyer et al., 2018), thus reducing some aspects of the processing requirement. We also processed images from 2000 to 2010 which have been documented in previous study (Li et al., 2012), to extend our analysis to a longer temporal coverage. Images of before and after flooding season in April and October were analysed every year. To achieve more accurate results, the selection of the satellite images was based on the following criteria: (1) lowest cloud coverage near the study area, (2) relatively closer date of the image acquisition for each year, and (3) similar tidal phase during the image acquisition.

In this study, we eventually utilized 45 satellite images obtained from the United States Geological Survey website (https://www.usgs.gov). In order to convert radiometric data to the above-water surface remote sensing reflectance data, the FLAASH atmospheric correction module from Environment for Visualizing Images (ENVI) was used to radiometric calibrate and atmospheric correct the obtained images. In term of the advanced image segmentation, eCognition 10.3 allows for the identification and delineation of different land cover features, including the coastline, by analysing spectral, spatial, and textural information from remote sensing images. Image segmentation is a crucial step in coastline analysis, as it allows for the accurate extraction of coastal boundaries (Dellepiane et al., 2004).

2.3 Modified normalized difference water index

When analysing the state of coastlines using remote sensing data, the primary objective is to extract the coastline within a specified timeframe, taking into account the factors such as tides to understand the coastline's variability and to identify the instantaneous waterline. The methodologies for automatically delineating the water's edge from remote sensing imagery are classified into edge detection, thresholding, and image classification techniques.

Recognizing the challenge of identifying the water boundary in areas with massive tidal flats, we introduced a modified Normalized Difference Water Index (NDWI). The conventional NDWI is based on the green and near-infrared bands, which can be less effective in regions with extensive tidal flats. In our research, we adopt a modified NDWI approach. Our modification incorporates additional bands or spectral indices to better differentiate between water and non-water surfaces in such areas. This methodology provides superior precision and resolution, enabling the detection of small-scale coastline changes.

In this study, modified NDWI utilizes the differences in reflectance between water and land in multi-spectral imagery to identify coastal areas (Bijeesh and Narasimhamurthy, 2020). Modified NDWI was refined by substituting NIR (0.76-0.90 μm) band in the original NDWI with the Short-Wave Infrared (SWIR1) band:

$$MNDWI = \frac{Green - SWIR1}{Green + SWIR1} \quad (1)$$

where the Green spectral band is 0.525 ~0.600 μm, and SWIR1 (1.560 ~1.660 μm) corresponds to the Short-Wave Infrared first band. Due to the similarity in the reflectance characteristics of water bodies and land cover, such as building area, in the NIR band and their significant differences in the SWIR1 band, the modified NDWI proves more effective in eliminating noise from tidal flat and building area.

In most cases, modified NDWI can better reveal the fine characteristics of water body by using SWIR1 band instead of NIR band used in NDWI, it can distinguish water bodies more easily and solve the problem that shadow noise is difficult to eliminate in water extraction. The previous studies have shown that modified NDWI is more suitable for enhancing water information than NDWI, and can extract water bodies more accurately (Du et al., 2014; Singh et al., 2015). In terms of accuracy, the Kappa coefficient of water extraction using modified NDWI was 0.0433 to 0.1348 higher than that using NDWI (Xu, 2006). Compared with NDWI, modified NDWI can better distinguish water from non-water from satellite images to extract coastline data.

2.4 Coastline change analysis workflow

By applying thresholding techniques to modified NDWI calculations, accurate coastline boundaries can be extracted from remote sensing images. Thereafter, the Digital Shoreline Analysis System (DSAS) was applied to analyse coastline positions over time. Coastline erosion or accretion rates could be calculated by the DSAS, which enables the assessment of the impact of erosion and siltation on coastal coastlines in coastal areas using remote sensing data (Quang et al., 2021). By overlaying different temporal datasets and employing spatial analysis tools, the coastal features over time along the coastline could be examined. The DSAS module consists of five steps: (1) coastline extraction; (2) baseline creation, where the baseline is created using a buffer method with the same curved shape as the nearest coastline; (3) generation of cross-shore profiles by defining intervals and orthogonally projecting the cross-shore profiles onto different-year coastlines after multiple adjustments; (4) calculation of the distance between the baseline and coastline; (5) calculation of coastline change rates. The End Point Rate (EPR) and Net Shoreline Movement (NSM) models are applied to calculate the rates using adjacent coastlines. EPR and NSM are essential tools for analysing coastline changes. EPR focuses on the rate of change over time, providing a temporal perspective, while NSM offers a spatial perspective by quantifying the total movement of the shoreline. In addition, NSM is used to measure long-term net coastline changes between 2000 and 2020, while EPR displays the annual rate of change during the mentioned period. Together, they offer a robust framework for understanding and managing coastal environments. The calculation method for EPR is as below:

$$E_{i,j} = \frac{d_j - d_i}{\Delta Y_{j,i}} \quad (2)$$

where $E_{i,j}$ represents the rate of change in the coastline endpoint along a certain baseline from one period to another; d_j is the distance from the coastline in the j period along line to the

baseline; *di* is the distance from the coastline in the *i* period along line to the baseline; and $\triangle Y_{j,i}$ is the difference in years between the *j* and *i* coastline periods. The workflow of the coastline change analysis in this study is demonstrated in Figure 2.

3 Results and discussion

3.1 Coastline changes under anthropogenic impacts

Our analysis of Landsat images revealed significant coastline changes in the YRE from 2010 to 2020. The changes were categorized into erosion and accretion, which were further correlated with environmental and anthropogenic factors. Human activities, such as land reclamation and construction of harbours, were identified as key contributors to coastline changes.

Coastal human structures can induce two primary phenomena: 1) modifications in pre-existing hydrodynamic conditions; and 2) a rapid seaward advancement of the coastline, resulting in significant changes to the coastline, a reduction in sea area, and a decrease in the amount of water accommodated by the tide. Engineering projects that intersect the tidal current at an angle can induce deflection of flow, altering the direction of the current, and may even create flows along the embankment that are nearly perpendicular to the original current direction. This is particularly pronounced when the velocity of the incoming tide exceeds that of the outgoing tide, leading to enhanced sediment accumulation and tidal flat siltation. Consequently, they alter the sedimentary balance affecting the shoreline, leading to coastal erosion and accretion.

Over the past decade, there has been an escalating trend in the utilization of the YRE's coastline, with a notable increase in the diversity of artificial coastline types (Figure 3). We extract the coastline in spring to eliminate the influence from the wet season. While some sections of the YRE's coastal dynamics exhibit subtle changes. However, there are notable spatial distribution changes in certain areas, which may be attributed primarily to the region's coastal composition, predominantly of bedrock and silt coastlines. The relative stability of bedrock sections is higher, whereas the silt coastlines exhibit less stability.

From 2010 to 2020, the Yalu River's coastline maps reveal a notable changing trend (Figure 4). Comparing the change pattern of the estuarine coastline from 2010 to 2014, a noticeable expansion of artificial coastlines is evident in the Donggang City area, with clear differences. Additionally, there is an increased presence of islands in the south-eastern region. During this period, the overall area of the YRE coastline increased, primarily due to the construction of coastal artificial structures. Since 2014, there has been a substantial increase in the extent of artificial coastlines in the YRE basin. These artificial constructs encompass various features such as aquaculture embankments, tidal barriers, salt fields, and port terminals. This transition highlights the diminishing spatial footprint of natural coastlines within the region. By comparing the spatiotemporal changes in the southern coastline segments between 2014 and 2020, it can be observed that the coastal area has also increased in size in 2020, mainly due to land reclamation projects, leading to an increase in land area. This is closely related to a series of local coastline protection policies and the implementation of various coastal land reclamation projects.

In general, the estuarine area has expanded in 2020, compared to 2010, but there is a certain degree of erosion observed in the area

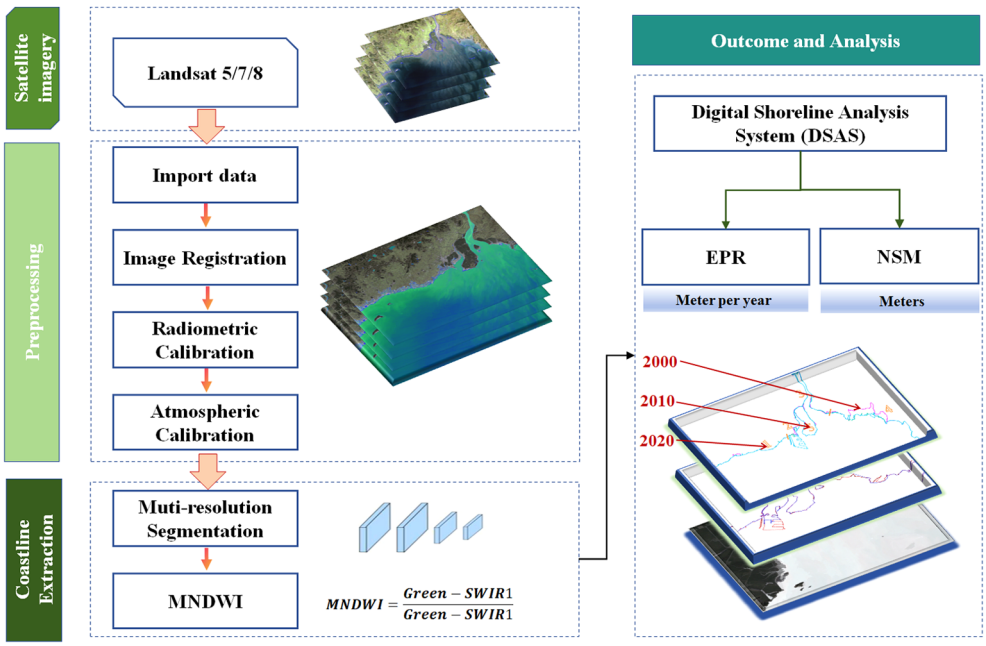

FIGURE 2
The applied methods for the extraction of coastline changes in this study.

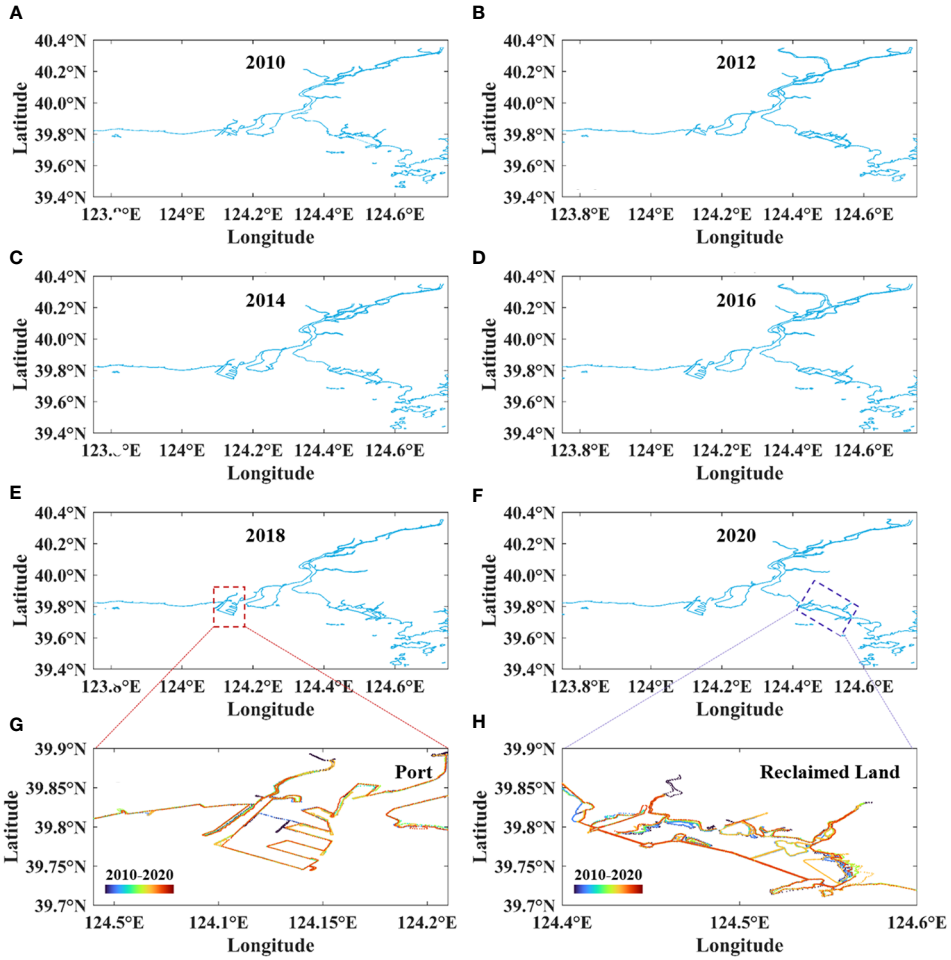

FIGURE 3
(A–F) the distribution of coastline from 2010 to 2020, **(G)** the coastline of port from 2010 to 2020, **(H)** the coastline of reclaimed land from 2010 to 2020.

near the mouth of the Yalu River, accompanied by a year-on-year reduction in the island areas at the estuarine mouth.

To elucidate the spatiotemporal characteristics of the YRE coastline changes more effectively, this study segmented the research area into five distinct sections: S1, S2, S3, S4, and S5 (Figure 5A). The coastline changing trends for each period are summarised in Table 1. Section S1 encompasses the western aquaculture sector of the YRE. Section S2 includes the Dandong port construction area. Section S3 is designated as the inner estuary region, and Section S4 constitutes the eastern bank of the YRE.

Between the years 2000 and 2010, the YRE coast exhibited spatial transformations, with the spatial distribution of the EPR depicted in Figure 5B. According to these results, during the decade of 2000-2010, there was a general trend of accretion along the YRE coastline. A breakdown by sector revealed that section S1 and S2 experienced modest accretion, with average NSM of 74.4 m and 335.62 m, respectively. The highest rate of accretion was noted in section S2 at 134.19 m per year, while the maximum erosion rate occurred in section S1 at 55.46 m per year. In section S3, coastal changes were relatively mild, but the overarching trend was still one of accretion. The most significant changes were recorded in section S4, which had a maximum accretion rate of 549.16 m per year, and an average NSM of 1205.45 m.

During the period from 2010 to 2020, the coastal areas of the YRE, particularly in section S1 and S2, exhibited patterns of sediment accumulation (Figure 5B). Section S1 maintained a relatively stable condition with only minor accretion observed. In contrast, section S2 underwent the most dramatic changes, with the highest accumulation rate recorded at 784.77 m per year and an average net coastline accretion amounting to 1071.88 m. Section S3 displayed a trend towards slight erosion overall, with the maximum erosion rate reaching 117.18 m per year and an average net erosion of the coastline being 74.24 m. Similarly, section S4 also experienced marginal erosion with the maximum erosion rate at 56.37 m per year and an average net coastline erosion totalling 21.04 m.

Between the years 2000 and 2020, the overall coastline of the YRE displayed a trend of accretion (Figure 5B). However, the temporal and spatial distribution of the EPR was heterogeneous.

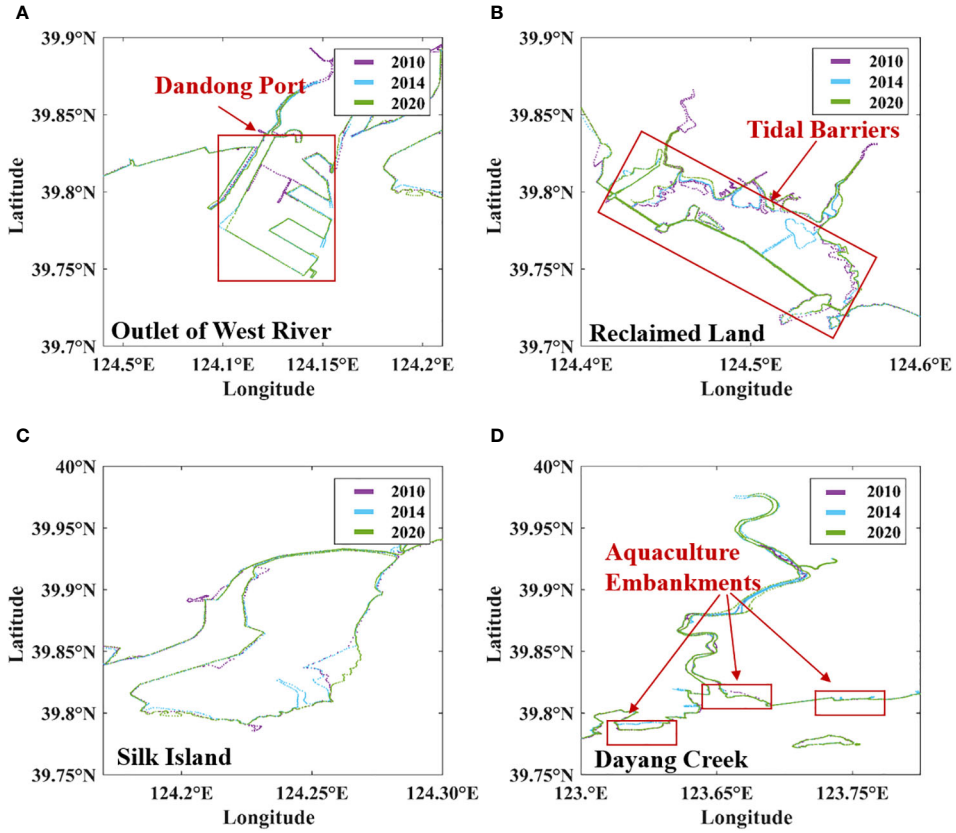

FIGURE 4
The changes of the coastline due to the anthropogenic activities in 2010, 2014 and 2020, **(A)** the local port area, **(B)** the reclaimed land region, **(C)** the silk island, and **(D)** the local Dayang creek.

With the comparison of all sections, S3 (the inner estuary) showed minor erosive tendencies, with the highest erosion rate being 57.05 m per year and an average net coastline erosion of 38.37 m. The other sections exhibited accretion, with particularly noticeable contributions to coastline growth from the construction activities in the local Port area (S2) and land reclamation in section S4. Moreover, S5 (the sandy island) experienced slight erosion throughout the 2000-2020 period, with the maximum erosion rate at 24.99 m per year and an average net coastline erosion amounting to 52.49 m.

The alterations in the length of the YRE coastline from 2000 to 2020 are summarised in Table 2. It is evident from the table that over the past two decades, the total coastline length across sections S1 to S4 has demonstrated an increasing trend, with an extension of approximately 59 km. This increment corresponds to a 22.6% surge, with an annual average growth rate of 2.95 km per annum. The most significant change occurred between 2010 and 2020, during which the coastline length expanded by 49.3 km. Examining the changes by section, during 2000-2020, the coastline of section S2 experienced a growth of 396.9% due to the construction activities in Dandong Port. Consequently, it is apparent that the primary contributor to the change in the YRE's coastline length during 2000-2020 was the increase in artificial coastline resulting from the development of local Port.

3.2 Impacts of natural processes on coastline change

In recent years, the occurrence of extreme weather has accelerated the coastline change of the estuarine region, with flooding events caused by extreme rainfall having a severe impact on the estuarine landscape (Cooper, 2002; Xie et al., 2018; Du et al., 2023). Even just one strong flooding can induce dramatic changes in the estuarine landscape (Dittmann et al., 2015; Ward et al., 2018).

In August 2010, the Yalu River basin experienced a severe flooding event (recurring every 50 years) caused by subtropical high pressure (Du et al., 2023). Intense rainfalls reached the catchment on 19th August 2010, resulting in a peak discharge of 12,800 m^3/s at Huanggou Hydrological Station (Figure 6), the Huanggou hydrological Station is in the lower reaches of the Yalu River, with a catchment area of 55,420 km^2. Analysing the monthly sediment transport, runoff, and precipitation data of the Yalu River reveals the following trends. In 2010, the river's sediment load reached its peak, coinciding with the highest monthly average precipitation. When examining the overall trend, the average runoff in 2010 reached its maximum in August, accompanied by the peak precipitation in the area. This indicates that, in 2010, precipitation was the predominant factor influencing river runoff in the region. The increase in precipitation contributed to the expansion of the YRE area. In 2013, despite relatively high rainfall, the

10.3389/fmars.2023.1335064

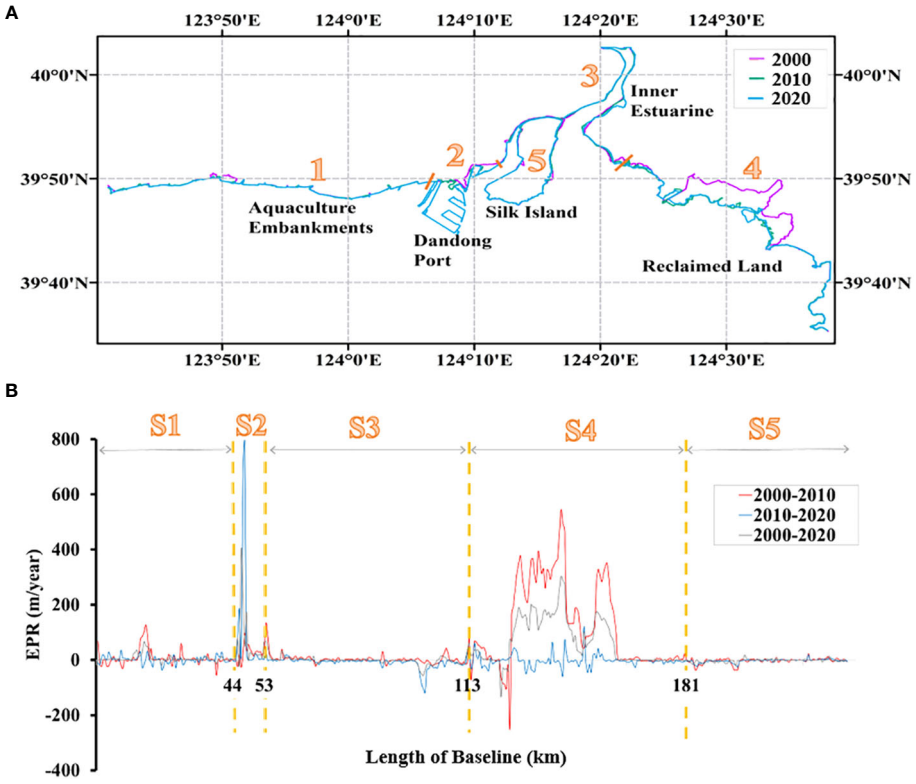

FIGURE 5
(A) the division of the coastline into 5 sections in YRE, and **(B)** the EPR for each section.

TABLE 1 The coastline summary of each section.

Time	Section	Variation length (km)	Average EPR ($m \cdot a^{-1}$)	Max Accumulation EPR ($m \cdot a^{-1}$)	Max Erosion EPR ($m \cdot a^{-1}$)	Average NSM (m)
2000 | 2010	S1	4.5	7.37	127.65	55.46	74.4
	S2	13	33.24	134.19	27.53	335.62
	S3	-1.6	2.47	80.38	22.6	24.94
	S4	-2.4	119.4	549.16	103.88	1205.45
	S5	-1	-2.63	22.79	37.72	-26.5
2010 | 2020	S1	-2.2	1.79	35.7	35.35	16.92
	S2	49.3	112.83	787.44	4.29	1071.88
	S3	2.1	-7.65	43.11	117.18	-72.24
	S4	-3.7	-2.33	122.35	56.37	-21.04
	S5	1	-2.58	17.63	20.8	-29.47
2000 | 2020	S1	2.3	5.06	65.41	19.56	98.89
	S2	62.3	68.51	395.4	14.84	1338.45
	S3	0.5	-1.96	60.81	57.05	-38.37
	S4	-6.1	65.63	302.58	134.25	1282.2
	S5	0	-2.44	19	24.99	-52.49

10.3389/fmars.2023.1335064

TABLE 2 The length of coastlines and growth rate of the sections from 2000 to 2020.

	S1-S4(km)	Growth Rate (%)	S2(km)	Growth Rate (%)	S5(km)	Growth Rate (%)
2000 | 2010	260.7 | 274.2	5.2	15.7 | 28.7	82.8	55.6 | 55.2	0
2010 | 2020	274.2 | 319.7	16.7	28.7 | 78	171.8	55.2 | 55.6	-0.7
2000 | 2020	260.7 | 319.7	22.6	15.7 | 78	396.9	| 55.6	0

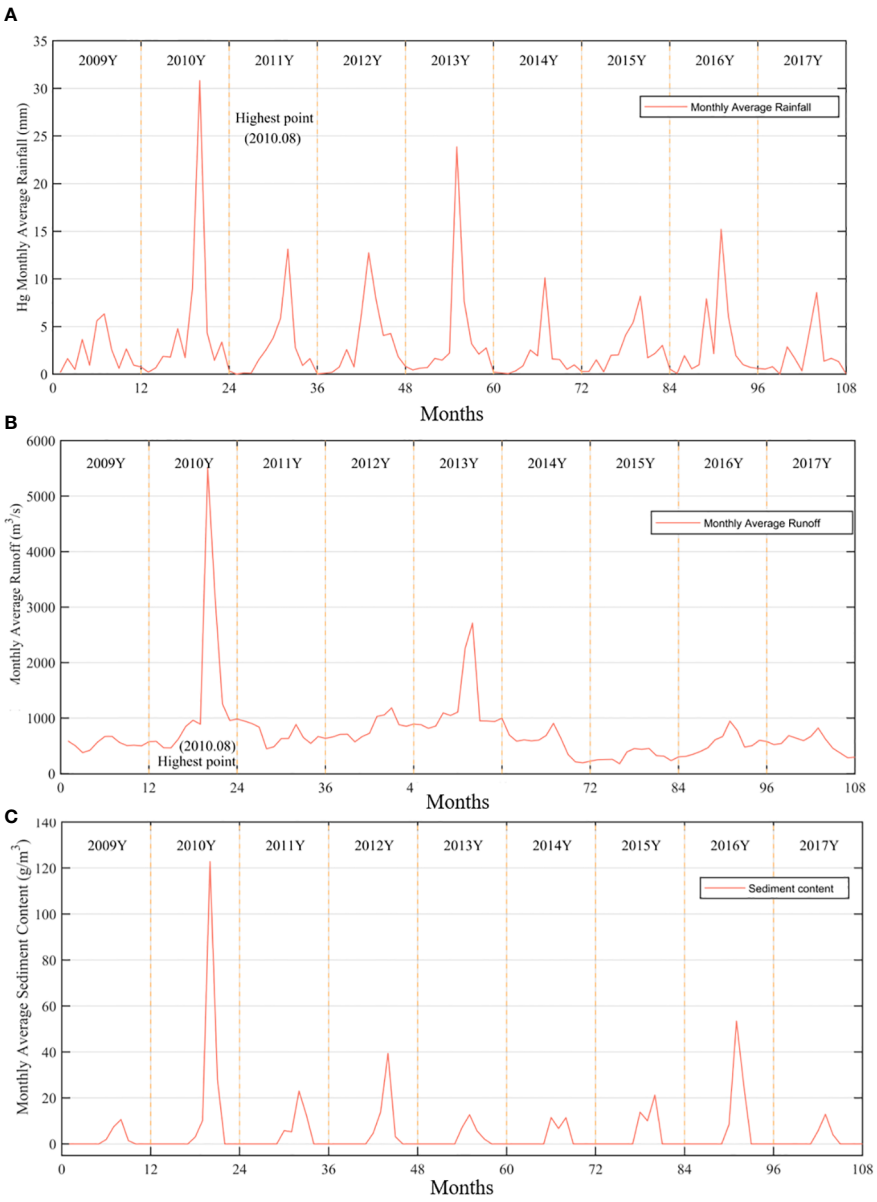

FIGURE 6
The monitoring data from 2009 to 2017, **(A)** the monthly average precipitation, **(B)** monthly average runoff, and **(C)** monthly average sediment discharge at the hydrological measurement station in the Yalu River basin.

sediment transport remained stable, leading to a minor peak in the YRE's runoff for that year. Estuarine sediments are mainly from two sources: terrigenous sediments discharged by rivers and flood events, and neritic sediments, including the local resuspended sediments from the seabed. Driven by extreme flooding caused by heavy rains in 2010, sediment content in YRE increased dramatically (Figure 6C), resulting in a significant expansion of the coastline in the fall of 2010. Flood events often carry significant amounts of sediments from inland areas to the coast. The volume, composition, and grain size of these sediments can vary greatly between events, directly influencing the nature of coastline changes. For instance, heavier sediment loads can lead to rapid buildup of the coastline, while finer sediments might be easily redistributed by tidal and wave actions, leading to more subtle changes. In areas with higher sediment deposition, this can lead to the formation of new landforms like sandbars or deltas, significantly altering the coastal landscape.

After the flood season, the runoff basin area of the Yalu River in 2010 autumn was significantly larger than that of 2010 spring. Compared to the previous year, the number of tributaries of the Yalu River increased slightly, which may be related to local precipitation. During the same period, the coastline area of the YRE is expected to increase, reflecting a certain trend of coastal accumulation, such as Silk Island and eastern bank of YRE. Land areas were slightly increased compared to the previous year, while the length of the estuary continued to expand (Figures 7A, B).

Furthermore, when comparing the spatial and temporal distribution characteristics of the YRE coastline in 2013 and 2010 during spring season, it can be observed that the pattern in the estuary region in 2013 is similar to that in 2010. From this, it can be inferred that the changes in the YRE are significant but overall in a dynamic balance. This may be related to local precipitation and sediment transport, as these two factors have interacted over the long term, resulting in cyclic changes in the size of the coastline segments in the region, with no significant overall trend.

Comparing seasonal variation in 2013 with the second highest runoff in the past decade, it is evident that in autumn 2013, the western river's basin area in this region increased (Figures 7C, D). From images of the following years, this pattern in the West Channel in this region remained stable, indicating that this change is persistent and stable, with distinct characteristics.

Furthermore, the distributions of coastline in spring for the year of 2010, 2012 and 2014 are illustrated in Figure 8. Comparative analysis can find that the area of the coastline has generally increased, and the increased coastline types are mainly artificial coastlines. In addition to the increase in artificial shorelines, there is also an increase in the estuary bank area caused by partial sediment accumulation at the estuary. This is usually related to the amount of sediment and rainfall in the area during the flood events. Changes in hydrological conditions and sediment load are significant factors in the YRE coastline changes. The YRE is a land-sea bidirectional

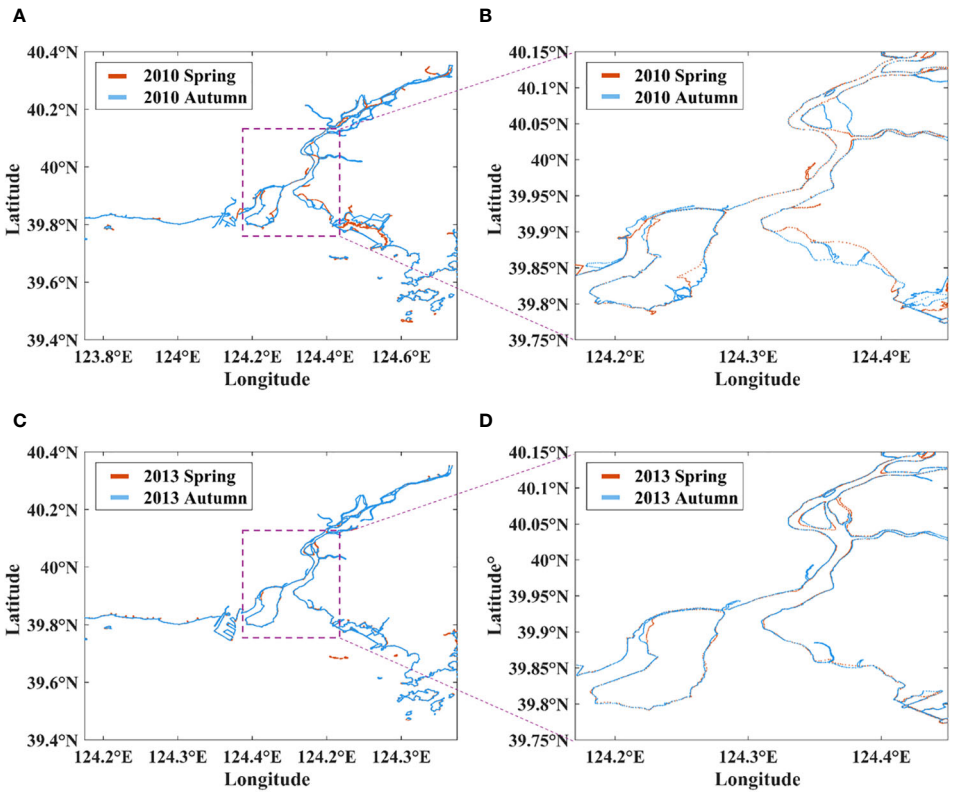

FIGURE 7
The distribution of coastline in spring and autumn for the year of 2010 and 2013, **(A)** overall shoreline of YRE in spring and autumn 2010, **(B)** partial shoreline of YRE in spring and autumn 2010, **(C)** overall shoreline of YRE in spring and autumn 2013, **(D)** partial shoreline of YRE in spring and autumn 2013.

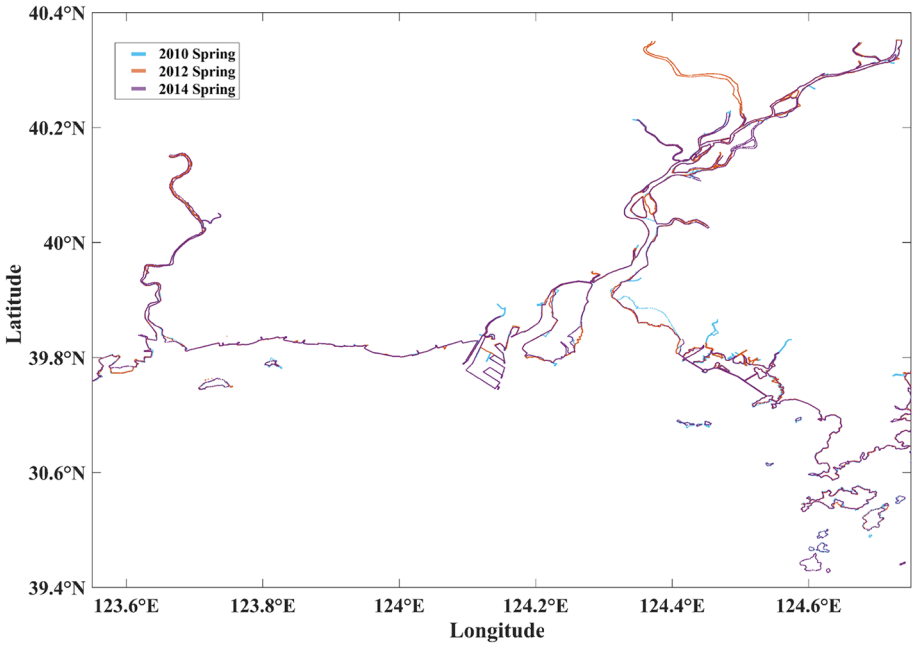

FIGURE 8
The coastline distribution in spring for the year of 2010, 2012 and 2014.

estuary type, with abundant terrestrial and marine sediments in the region. Under the influence of waves and tides, nearshore sediments will eventually accumulate on land or flow into the ocean with the tide, leading to coastline migration.

4 Conclusion

This study summarizes the causes of YRE coastline changes, mainly divided into anthropogenic and natural factors. On the anthropogenic side, the construction of aquaculture areas and embankments is the main project for artificial coastline construction and is a major influencing factor for coastline expansion. Due to the construction of a large number of artificial hydraulic structures, the morphology changes along the YRE have been greatly affected, with an increase of 22.6% from 2000 to 2020 for S1-S4. In addition, the prevalence of land reclamation in recent years is also an important factor restricting changes in the coastline. Regarding natural factors, the differences in hydrological conditions and sediment transport of the areas of aquaculture and embankments have led to inconsistent rates of coastal erosion.

This study shows that from 2010 to 2020, the YRE coastline changes were quite significant, indicating a shift from a phase of expansion to erosion. The YRE and its downstream channels eventually expanded towards both banks, with numerous riverbed islands forming. Analysis reveals that human activities and alternations in hydrological conditions are important factors affecting the YRE coastline changes, contributing to the formation of distinctive spatiotemporal patterns.

The findings highlight the complex interplay between natural and anthropogenic factors in shaping the coastal environment. The observed coastline changes in the YRE have significant implications for the region. Erosion can lead to loss of habitat and infrastructure damage, while accretion can impact navigational routes and submarine groundwater discharge. It is essential to balance economic development with environmental conservation to ensure the long-term sustainability of the estuary ecosystem. Future research should focus on predictive modelling and integrated coastal zone management to address the challenges posed by coastline changes in this unique estuarine ecosystem.

Data availability statement

The original contributions presented in the study are included in the article/supplementary material. Further inquiries can be directed to the corresponding author.

Author contributions

QW: Software, Validation, Writing – original draft. YM: Conceptualization, Data curation, Writing – review & editing. ZC: Funding acquisition, Methodology, Software, Visualization, Writing – review & editing. YD: Visualization, Writing – review & editing.

Funding

The author(s) declare financial support was received for the research, authorship, and/or publication of this article. This study

was funded by the National Key Research and Development Program of China (Grant No. 2021YFB2601100), the National Natural Science Foundation of China (Grant No. 52201309, 42276170, 42106158), and the Fundamental Research Funds for the Central Universities (Grant No. 3132023158).

Acknowledgments

The Landsat images utilized in this study were sourced from the United States Geological Survey (USGS) website. We would also acknowledge the support from Liaodong University for the great help in field observation.

Conflict of interest

The authors declare that the research was conducted in the absence of any commercial or financial relationships that could be construed as a potential conflict of interest.

Publisher's note

References

Alesheikh, A. A., Ghorbanali, A., and Nouri, N. (2007). Coastline change detection using remote sensing. *Int. J. Environ. Sci. Technol.* 4, 61–66. doi: 10.1007/BF03325962

Bai, F., Gao, J., Wang, Y., Cheng, Y., and Lin, T. (2008). Tidal characteristics at yalu river estuary. *Mar. Sci. Bull.* 27, 7–13.

Barbier, E. B., Hacker, S. D., Kennedy, C., Koch, E. W., Stier, A. C., and Silliman, B. R. (2011). The value of estuarine and coastal ecosystem services. *Ecol. Monogr.* 81 (2), 169–193. doi: 10.1890/10-1510.1

Bianchini, A., Cento, F., Guzzini, A., Pellegrini, M., and Saccani, C. (2019). Sediment management in coastal infrastructures: Techno-economic and environmental impact assessment of alternative technologies to dredging. *J. Environ. Manage.* 248, 109332. doi: 10.1016/j.jenvman.2019.109332

Bijeesh, T., and Narasimhamurthy, K. (2020). Surface water detection and delineation using remote sensing images: A review of methods and algorithms. *Sustain. Water Resour. Manage.* 6, 1–23. doi: 10.1007/s40899-020-00425-4

Cheng, Z., Jalon-Rójas, I., Wang, X. H., and Liu, Y. (2020). Impacts of land reclamation on sediment transport and sedimentary environment in a macro-tidal estuary. *Estuarine. Coast. Shelf. Sci.* 242, 106861. doi: 10.1016/j.ecss.2020.106861

Cheng, Z., Wang, X. H., Jalon-Rojas, I., and Liu, Y. (2019). Reconstruction of sedimentation changes under anthropogenic influence in a medium-scale estuary based on a decadal chronological framework. *Estuarine. Coast. Shelf. Sci.* 227, 106295. doi: 10.1016/j.ecss.2019.106295

Cheng, Z., Wang, X. H., Paull, D., and Gao, J. (2016). Application of the geostationary ocean color imager to mapping the diurnal and seasonal variability of surface suspended matter in a macro-tidal estuary. *Remote Sens.* 8 (3), 244. doi: 10.3390/rs8030244

Cooper, J. (2002). The role of extreme floods in estuary-coastal behaviour: contrasts between river-and tide-dominated microtidal estuaries. *Sediment. Geol.* 150 (1-2), 123–137. doi: 10.1016/S0037-0738(01)00271-8

Dellepiane, S., De Laurentiis, R., and Giordano, F. (2004). Coastline extraction from SAR images and a method for the evaluation of the coastline precision. *Pattern Recognition. Lett.* 25 (13), 1461–1470. doi: 10.1016/j.patrec.2004.05.022

Dittmann, S., Baring, R., Baggalley, S., Cantin, A., Earl, J., Gannon, R., et al. (2015). Drought and flood effects on macrobenthic communities in the estuary of Australia's largest river system. *Estuarine. Coast. Shelf. Sci.* 165, 36–51. doi: 10.1016/j.ecss.2015.08.023

Du, Y., Cheng, Z., and You, Z. (2023). Morphological changes in a macro-tidal estuary during extreme flooding events. *Front. Mar. Sci.* 9, 1112494. doi: 10.3389/fmars.2022.1112494

Du, Z., Li, W., Zhou, D., Tian, L., Ling, F., Wang, H., et al. (2014). Analysis of Landsat-8 OLI imagery for land surface water mapping. *Remote Sens. Lett.* 5, 672–681. doi: 10.1080/2150704X.2014.960606

Dwyer, J. L., Roy, D. P., Sauer, B., Jenkerson, C. B., Zhang, H. K., and Lymburner, L. (2018). Analysis ready data: enabling analysis of the landsat archive. *Remote Sens.* 10, 1363. doi: 10.3390/rs10091363

Gao, J.-h., Jun, L., Harry, W., Bai, F.-l., Cheng, Y., and Wang, Y.-p. (2012). Rapid changes of sediment dynamic processes in Yalu River Estuary under anthropogenic impacts. *Int. J. Sediment. Res.* 27 (1), 37–49. doi: 10.1016/S1001-6279(12)60014-6

Hapke, C. J., Kratzmann, M. G., and Himmelstoss, E. A. (2013). Geomorphic and human influence on large-scale coastal change. *Geomorphology* 199, 160–170. doi: 10.1016/j.geomorph.2012.11.025

Li, L., Zhang, J., Ma, Y., and Cui, X. (2012). Monitoring the coastline change in the Yalu River Estuary from 1976 to 2010 based on remote sensing images. *Bull. Surv. Mapp.* 386, 390.

Morgan, G. R., and Hodgson, M. E. (2021). A post-classification change detection model with confidences in high resolution multi-date sUAS imagery in coastal south carolina. *Int. J. Remote Sens.* 42 (11), 4309–4336. doi: 10.1080/01431161.2021.1890266

Muttitanon, W., and Tripathi, N. K. (2005). Land use/land cover changes in the coastal zone of Ban Don Bay, Thailand using Landsat 5 TM data. *Int. J. Remote Sens.* 26 (11), 2311–2323. doi: 10.1080/01431160512331326666

Quang, D. N., Ngan, V. H., Tam, H. S., Viet, N. T., Tinh, N. X., and Tanaka, H. (2021). Long-term shoreline evolution using dsas technique: a case study of Quang Nam province, Vietnam. *J. Mar. Sci. Eng.* 9, 10, 1124. doi: 10.3390/jmse9101124

Quiñones, R. A., Fuentes, M., Montes, R. M., Soto, D., and León-Muñoz, J. (2019). Environmental issues in Chilean salmon farming: a review. *Rev. Aquacult.* 11 (2), 375–402. doi: 10.1111/raq.12337

Roy, D. P., Zhang, H. K., Ju, J., Gomez-Dans, J. L., Lewis, P. E., Schaaf, C. B., et al. (2016). A general method to normalize Landsat reflectance data to nadir BRDF adjusted reflectance. *Remote Sens. Environ.* 176, 255–271. doi: 10.1016/j.rse.2016.01.023

Sahin, G., Cabuk, S. N., and Cetin, M. (2022). The change detection in coastal settlements using image processing techniques: a case study of Korfez. *Environ. Sci. pollut. Res.* 29 (10), 15172–15187. doi: 10.1007/s11356-021-16660-x

Sánchez-Arcilla, A., García-León, M., Gracia, V., Devoy, R., Stanica, A., and Gault, J. (2016). Managing coastal environments under climate change: Pathways to adaptation. *Sci. Total. Environ.* 572, 1336–1352. doi: 10.1016/j.scitotenv.2016.01.124

Shi, Y., Liu, Z., Gao, J., Yang, Y., and Wang, Y. (2017). The response of sedimentary record to catchment changes induced by human activities in the western intertidal flat of Yalu River Estuary, China. *Acta Oceanol. Sin.* 36, 54–63. doi: 10.1007/s13131-016-0941-7

Singh, K. V., Setia, R., Sahoo, S., Prasad, A., and Pateriya, B. (2015). Evaluation of NDWI and MNDWI for assessment of waterlogging by integrating digital elevation model and groundwater level. *Geocarto. Int.* 30, 650–661. doi: 10.1080/10106049.2014.965757

Tian, H., Xu, K., Goes, J. I., Liu, Q., and H.d.R. and Yang, M. (2020). Shoreline changes along the coast of mainland China—time to pause and reflect? *ISPRS. Int. J. Geo-Information.* 9 (10), 572. doi: 10.3390/ijgi9100572

Turner, R. K., Lorenzoni, I., Beaumont, N., Bateman, I. J., Langford, I. H., and McDonald, A. L. (1998). Coastal management for sustainable development: analysing environmental and socio-economic changes on the UK coast. *Geographical. J.* 164 (3), 269–281. doi: 10.2307/3060616

Ward, P. J., Couasnon, A., Eilander, D., Haigh, I. D., Hendry, A., Muis, S., et al. (2018). Dependence between high sea-level and high river discharge increases flood hazard in global deltas and estuaries. *Environ. Res. Lett.* 13 (8), 084012. doi: 10.1353/book.99575

Xie, D., Pan, C., Gao, S., and Wang, Z. B. (2018). Morphodynamics of the Qiantang Estuary, China: Controls of river flood events and tidal bores. *Mar. Geol.* 406, 27–33. doi: 10.1016/j.margeo.2018.09.003

Xu, H. (2006). Modification of normalised difference water index (NDWI) to enhance open water features in remotely sensed imagery. *Int. J. Remote Sens.* 27, 3025–3033. doi: 10.1080/01431160600589179

Xu, Y., Cheng, L., Zheng, J., Zhu, Y., Wu, Y., Shi, J., et al. (2019). Intensive anthropogenic influence on the morphological evolution of estuarine tidal channels. *J. Coast. Res.* 35 (6), 1237–1249. doi: 10.2112/JCOASTRES-D-18-00136.1

Yu, Q., Wang, Y., Gao, J., Gao, S., and Flemming, B. (2014). Turbidity maximum formation in a well-mixed macrotidal estuary: The role of tidal pumping. *J. Geophys. Res. Ocean.* 119, 7705–7724. doi: 10.1002/2014JC010228

Zhang, T., Yang, X., Hu, S., and Su, F. (2013). Extraction of coastline in aquaculture coast from multispectral remote sensing images: Object-based region growing integrating edge detection. *Remote Sens.* 5 (9), 4470–4487. doi: 10.3390/rs5094470

Zhu, Z., Fu, Y., Woodcock, C. E., Olofsson, P., Vogelmann, J. E., Holden, C., et al. (2016). Including land cover change in analysis of greenness trends using all available Landsat 5, 7, and 8 images: A case study from Guangzhou, China, (2000–2014). *Remote Sens. Environ.* 185, 243–257. doi: 10.1016/j.rse.2016.03.036

Zhu, Q., Wang, Y. P., Gao, S., Zhang, J., Li, M., Yang, Y., et al. (2017). Modeling morphological change in anthropogenically controlled estuaries. *Anthropocene* 17, 70–83. doi: 10.1016/j.ancene.2017.03.001